PNAS RESEARCH ARTICLE | MICROBIOLOGY OPEN ACCESS

SARS-CoV-2 Mac1 is required for IFN antagonism and efficient virus replication in cell culture and in mice

Yousef M. Alhammad[a,1], Srivatsan Parthasarathy[a,1], Roshan Ghimire[b,1], Catherine M. Kerr[a], Joseph J. O'Connor[a], Jessica J. Pfannenstiel[a], Debarati Chanda[b], Caden A. Miller[b], Nathalie Baumlin[c], Matthias Salathe[c], Robert L. Unckless[a], Sonia Zuñiga[d], Luis Enjuanes[d], Sunil More[b], Rudragouda Channappanavar[b,2], and Anthony R. Fehr[a,2]

Edited by Karla Kirkegaard, Stanford University, Stanford, CA; received February 6, 2023; accepted June 30, 2023

Several coronavirus (CoV) encoded proteins are being evaluated as targets for antiviral therapies for COVID-19. Included in these drug targets is the conserved macrodomain, or Mac1, an ADP-ribosylhydrolase and ADP-ribose binding protein encoded as a small domain at the N terminus of nonstructural protein 3. Utilizing point mutant recombinant viruses, Mac1 was shown to be critical for both murine hepatitis virus (MHV) and severe acute respiratory syndrome (SARS)-CoV virulence. However, as a potential drug target, it is imperative to understand how a complete Mac1 deletion impacts the replication and pathogenesis of different CoVs. To this end, we created recombinant bacterial artificial chromosomes (BACs) containing complete Mac1 deletions (ΔMac1) in MHV, MERS-CoV, and SARS-CoV-2. While we were unable to recover infectious virus from MHV or MERS-CoV ΔMac1 BACs, SARS-CoV-2 ΔMac1 was readily recovered from BAC transfection, indicating a stark difference in the requirement for Mac1 between different CoVs. Furthermore, SARS-CoV-2 ΔMac1 replicated at or near wild-type levels in multiple cell lines susceptible to infection. However, in a mouse model of severe infection, ΔMac1 was quickly cleared causing minimal pathology without any morbidity. ΔMac1 SARS-CoV-2 induced increased levels of interferon (IFN) and IFN-stimulated gene expression in cell culture and mice, indicating that Mac1 blocks IFN responses which may contribute to its attenuation. ΔMac1 infection also led to a stark reduction in inflammatory monocytes and neutrophils. These results demonstrate that Mac1 only minimally impacts SARS-CoV-2 replication, unlike MHV and MERS-CoV, but is required for SARS-CoV-2 pathogenesis and is a unique antiviral drug target.

coronavirus | macrodomain | ADP-ribosylation | interferon | SARS-CoV-2

Coronaviruses (CoVs) belong to the family *coronaviridae* and possess a large, positive-sense RNA genome. The subfamily *coronavirinae* is further subdivided into α, β, γ, and δ-CoVs, though only the α and β-CoVs include viruses that infect humans. Prior to the 21st century, CoVs were predominantly known to cause mild respiratory disease in humans (1). However, with the emergence of SARS-CoV, MERS-CoV, and most recently SARS-CoV-2, it is now well established that CoVs are implicated in severe human respiratory conditions and are a serious threat to human health.

Coronavirus infectious disease (COVID-19) caused by SARS-CoV-2 is responsible for the pandemic that has resulted in over 6 million deaths worldwide (WHO). In individuals with severe COVID-19, SARS-CoV-2 induces a robust proinflammatory cytokine response, or cytokine storm, leading to the development of acute respiratory distress syndrome and in some cases multiple organ pathologies (2). Introduction of SARS-CoV-2 mRNA vaccines has drastically increased antiviral immunity and has reduced the fatality caused by SARS-CoV-2 (CDC). However, many elderly or immunocompromised people have ineffective responses to vaccines (3), and with the rate of emergence of new SARS-CoV-2 variants like Omicron (BA.2, BA.4, and BA.5), there is an urgent need to identify novel antiviral drugs. Currently, a few antiviral drugs such as Veklury (Remdesivir) (4, 5) and Lagevrio (molnupiravir) (5) both of which target the CoV polymerase (nsp12); and Paxlovid (nirmatrelvir and ritonavir) (6), which targets the main protease (nsp5), have been utilized in hospitals to treat COVID-19 patients under adverse conditions. However, it remains important to identify novel drug targets to expand the pool of anti-CoV therapies that will be needed to account for drug resistance, provide additional options for treatment, and better understand the replication processes of CoVs.

All CoVs encode a conserved set of 15 to 16 nonstructural proteins that direct the formation of the replication transcription complex and carry out the process of RNA transcription and replication, making these proteins important targets for antiviral therapies. While much progress has been made in identifying the functions of many of the nonstructural proteins, we still lack a complete understanding of how these proteins contribute to RNA replication and

Significance

All CoVs, including SARS-CoV-2, encode for a conserved macrodomain (Mac1) that counters host ADP-ribosylation. Prior studies with SARS-CoV and MHV found that Mac1 is required for pathogenesis, which has prompted the development of SARS-CoV-2 Mac1 inhibitors. However, development of these compounds into antivirals requires that we understand the degree to which SARS-CoV-2 lacking Mac1 replicates and causes disease in vitro and in vivo. Here, we found that SARS-CoV-2 containing a complete Mac1 deletion replicates normally in cell culture but induces an elevated IFN response, has reduced viral loads in vivo, and does not cause significant disease in mice. These results will provide a roadmap for testing Mac1 inhibitors, help identify Mac1 functions, and open additional avenues for coronavirus therapies.

Author contributions: Y.M.A., S.P., C.M.K., J.J.O., J.J.P., S.M., R.C., and A.R.F. designed research; Y.M.A., S.P., R.G., C.M.K., J.J.O., J.J.P., D.C., C.A.M., S.M., and R.C. performed research; Y.M.A., J.J.O., N.B., M.S., R.L.U., S.Z., and L.E. contributed new reagents/analytic tools; Y.M.A., S.P., R.G., C.M.K., J.J.O., J.J.P., R.L.U., S.M., R.C., and A.R.F. analyzed data; and S.P., R.C., and A.R.F. wrote the paper.

Competing interest statement: A.R.F. and R.C. were named as inventors on a patent filed by the University of Kansas.

This article is a PNAS Direct Submission.

[1]Y.M.A., S.P., and R.G. contributed equally to this work.

[2]To whom correspondence may be addressed. Email: rchanna@okstate.edu or arfehr@ku.edu.

This article contains supporting information online at https://www.pnas.org/lookup/suppl/doi:10.1073/pnas.2302083120/-/DCSupplemental.

Published August 22, 2023.

evasion of the host immune response. Nonstructural protein 3 (nsp3) is the largest nonstructural protein encoded in the CoV genome and consists of several modular protein domains. All CoV nsp3 proteins contain a ubiquitin-like domain, a nucleic acid binding domain, several transmembrane domains, a highly conserved Y domain, a papain-like protease (PLP) domain, and a conserved macrodomain (Fig. 1*A*). SARS-CoV and SARS-CoV-2 encode for 3 tandem macrodomains at the N terminus of nsp3 (Mac1, Mac2, and Mac3), with Mac2 and Mac3 being previously termed SUD-N and SUD-M. Mac1 is conserved throughout all CoVs, unlike Mac2 and Mac3, and has biochemical functions that are distinct from Mac2 and Mac3 (7–12). Notably, homologs of Mac1 are also found in other viruses like alphaviruses, hepatitis E virus, and rubella virus, suggesting that macrodomains could play an important role in the replication of a subset of positive-strand RNA viruses (13, 14). Biochemically, the conserved viral macrodomain binds to ADP-ribose moieties with high affinity (15, 16) and in some cases can hydrolyze the bond between ADP-ribose and proteins, reversing ADP-ribosylation, a common posttranslational modification (15, 17–20).

ADP-ribosylation is catalyzed by ADP-ribosyltransferases (ARTs/PARPs) using NAD^+ as the substrate (21). ADP-ribose subunits can be added to proteins as single subunits in a process termed mono-ADP-ribosylation (or MARylation) or as a polymer of ADP-ribose subunits forming a chain in a process termed poly-ADP-ribosylation (or PARylation). Notably, several of the MARylating PARPs are interferon-stimulated genes (ISGs) and demonstrate antibacterial and antiviral properties (22–25). These results highlight the importance of ADP-ribosylation as a putative antiviral host response and viral macrodomains as an evolutionary adaptation by certain viruses to counter this host response (17, 19, 20). Therefore, it is of interest to better understand how viral macrodomains counter PARP activity and contribute toward viral infection and pathogenesis.

The recent body of research has identified Mac1 as a viral factor necessary for CoV replication and pathogenesis in multiple animal models of infection (18, 26). Most of these studies have utilized a point mutant of Mac1 where a conserved asparagine residue (N1347 in MHV-JHM) was mutated to an alanine. This mutation dramatically reduces the ability of Mac1 to hydrolyze MAR from target proteins (16, 18, 27–29). The SARS-CoV Mac1 asparagine-to-alanine mutant virus (N1040A) had minimal to no impact on replication in transformed cells but was sensitive to IFN-I pretreatment and induced robust IFN and proinflammatory cytokine production and caused minimal disease in a mouse model of infection (18, 30). Similar results were seen with the corresponding MHV Mac1 mutant virus (N1347A), though growth defects have been observed in some cell types with this virus (31–33). Importantly, MHV N1347A replication increased upon PARP inhibition, while WT virus was unaffected. Similarly, IFN-I induction following infection with MHV N1347A was nearly eliminated upon PARP inhibition. These results indicate that Mac1 function countered the action of PARP-mediated ADP-ribosylation (32). Apart from N1347A, we found that another unique mutation, D1329A, a residue which is critical for the ADP-binding activity of macrodomains, replicated poorly in multiple cell types. Additionally, we were unable to recover an MHV double mutant virus, D1329A/N1347A, indicating that Mac1 may be critical for CoV replication. These results demonstrate that Mac1 has multiple functions that can promote viral replication and block host interferon responses (33).

These combined studies have prompted several groups to begin screening for and developing SARS-CoV-2 Mac1 inhibitors that could potentially be used therapeutically to treat patients infected with SARS-CoV-2 or other emerging CoVs (34–41). However, before testing any of these inhibitors for their antiviral activity, it is imperative to determine the role and functions of Mac1 in SARS-CoV-2 replication, pathogenesis, and the host immune response. Here, we have created a complete SARS-CoV-2 Mac1 deletion virus and characterized its replication and immune-modulating properties. These results provide insights into SARS-CoV-2 biology, the innate immune response to infection and will provide a roadmap for future testing of Mac1 inhibitors for antiviral activity.

Results

SARS-CoV-2 Mac1 Deletion Virus Infectious Virus Was Easily Recovered While Mac1 Deletion Viruses in other β-CoVs Were Not Recovered. We recently identified several Mac1 mutations in murine hepatitis virus strain JHM (MHV-JHM) that were unrecoverable from a bacterial artificial chromosome (BAC) based reverse genetic system (33). These results indicated that Mac1 may be critical for MHV replication. As point mutations

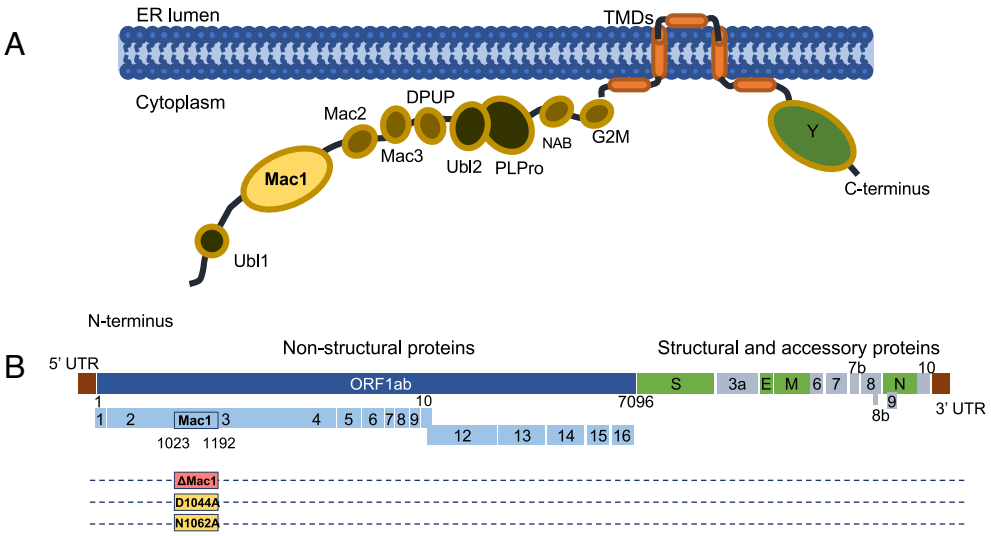

Fig. 1. SARS-CoV-2 nonstructural protein three domains and location of Mac1 in SARS-CoV-2 genome. (*A*) Cartoon diagram illustrating the different domains of SARS-CoV-2 nsp3. (*B*) Schematic of the SARS-CoV-2 genome with location of Mac1, indicating the area of the Mac1 deletion and the point mutations that were engineered.

could result in toxic unfolded proteins, we engineered a Mac1 deletion into the MHV-JHM BAC to confirm our prior results (Fig. 1*B*). As expected, we were unable to recover infectious virus (*SI Appendix*, Fig. S1 *A* and *B*) from the Mac1 deletion BAC, further indicating that Mac1 is critical for MHV-JHM replication. We next engineered a complete deletion of Mac1 into the MERS-CoV BAC, and again, we were unable to recover infectious virus, indicating that Mac1 is also critical for MERS-CoV replication (*SI Appendix*, Fig. S1 *A* and *B*). We hypothesized that Mac1 might be essential for the replication of all CoVs, so we engineered a Mac1 deletion (ΔMac1) into a SARS-CoV-2 BAC (Wuhan strain) to provide additional evidence for our hypothesis. However, unlike MHV-JHM or MERS-CoV, this virus was easily recoverable (*SI Appendix*, Fig. S1 *A* and *B*). This result indicates that there are stark differences in the requirement for Mac1 between SARS-CoV-2 and other β-CoVs.

SARS-CoV-2 ΔMac1 Replicates like WT Virus in Most Cell Types. Next, we assessed the ability of SARS-CoV-2 ΔMac1 to replicate in several cell types susceptible to SARS-CoV-2. In Vero E6 cells, ΔMac1 replicated like WT virus at both low (Fig. 2*A*) and high (*SI Appendix*, Fig. S2*A*) multiplicity of infection (MOI), indicating that Mac1 is not required for general virus replication. Vero E6 cells lack the ability to produce IFN-I, and MHV-JHM Mac1 mutant viruses are more attenuated in cells that maintain the ability to produce IFN-I (32). Thus, we hypothesized that SARS-CoV-2 ΔMac1 may be attenuated in either A549-ACE2 (alveolar epithelial cells) or Calu-3 cells (bronchial epithelial cells) that have a functional IFN system. ΔMac1 replicated equally to the WT virus in A549-ACE2 cells (Fig. 2*B*); however, there was an ~2- to 3-fold reduction in ΔMac1 titers in Calu-3 cells compared to the WT virus at both low (Fig. 2 *C* and *D*) and high MOI (*SI Appendix*, Fig. S2 *B* and *C*). We further observed only mild, if any, reduction

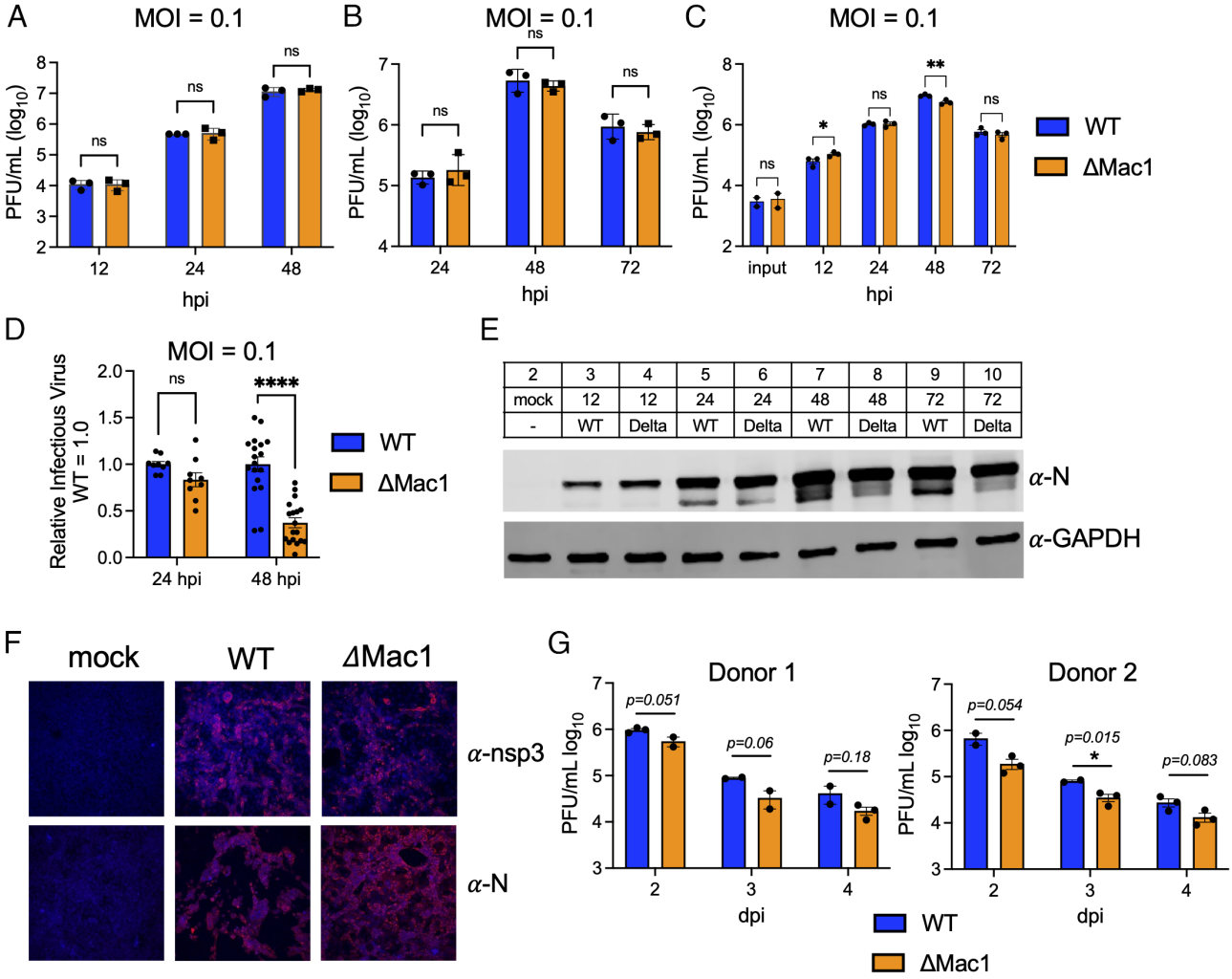

Fig. 2. SARS-CoV-2 ΔMac1 replicates normally in Vero E6 and A549 cells but has a mild replication defect in Calu-3 and primary epithelial cells. (*A* and *B*) Vero E6 (*A*) and A549-ACE2 (*B*) cells were infected with SARS-CoV-2 WT and ΔMac1 at an MOI of 0.1 PFU/cell. Both cell-associated and cell-free virus was collected at indicated time points and virus titers were determined by plaque assays. Data shown are one experiment representative of three independent experiments. $n = 3$ per group for each experiment. The data in *A* and *B* are from one experiment representative of at least three independent experiments. $n = 3$ per group. (*C* and *D*) Calu-3 cells were infected with SARS-CoV-2 WT and ΔMac1 viruses at low MOI. Both cell-associated and cell-free virus was collected at indicated times, and virus titers were determined by the plaque assay. The data in *C* are from one experiment representative of at least three independent experiments. $n = 3$ per group. (*D*) The results of all combined experiments from Calu-3 cells (*C*), where the average WT values from each experiment were normalized to 1.0 at 24 and 48 hpi are shown. Each point represents a separate biological replicate. (*E* and *F*) Calu-3 cells were infected at an MOI of 1 PFU/cell, and cell lysates were collected, and viral protein levels were determined by immunoblotting (*E*) or cells were fixed at 24 hpi were costained with DAPI and either anti-nsp3 or anti-N and then analyzed by confocal microscopy at 20× magnification (*F*). The data in *E* and *F* show data from one representative experiment of two independent experiments. (*G*) Primary human bronchial epithelial cells grown at air–liquid interface were infected apically with SARS-CoV-2 WT and ΔMac1 at an MOI of 0.2 (Donor 1) or 0.02 (Donor 2) PFU/cell. Cell-free virus was collected from the apical side at indicated time points and virus titers were determined by plaque assays. $n = 2$ to 3 per group for each experiment.

in viral N protein when analyzed by immunoblotting, and we observed roughly equal levels of both N protein and nsp3 staining by confocal microscopy (Fig. 2 *E* and *F*) in Calu-3 cells infected by WT and ΔMac1. Additionally, we evaluated the replication of these viruses in primary bronchial epithelial cells. Again, we found that ΔMac1 consistently produced 2- to 3-fold fewer infectious progeny virus from multiple donors, reaffirming the mild replication defect observed in Calu-3 cells (Fig. 2*G*).

To evaluate the relative fitness of ΔMac1 compared to WT virus, we performed a competition experiment where we coinfected Calu-3 cells with WT and ΔMac1 at ratios of 1:1 and 1:9, respectively, and followed these viruses over the course of four passages. Virus was collected at approximately 36 hpi after each passage to isolate virus during active replication, and not after peak replication has been reached. To distinguish between WT and ΔMac1 viruses, we used semiquantitative RT-PCR with primers set outside of Mac1 that produce different-sized PCR products from each virus. First, using BAC DNA, we found that the ratio of these bands correlated with the ratio of input BAC (*SI Appendix*, Fig. S3 *A* and *B*), indicating that this method could faithfully define the relative abundance of each virus following passaging. We found that after four rounds of passaging ΔMac1 had not been outcompeted by WT virus as the ratios of these two viruses stayed relatively stable over the entire experiment (*SI Appendix*, Fig. S3 *C* and *D*), though WT virus was starting to increase in abundance in the 9:1 (ΔMac1:WT) sample at passage four. In total, these results indicate that ΔMac1 generally replicates like WT virus but has a mild replication defect in Calu-3 cells.

SARS-CoV-2 ΔMac1 Is More Sensitive to IFN-γ Pretreatment than WT Virus. We previously found that IFN-β pretreatment more effectively reduced MHV Mac1 mutant virus replication than WT virus replication in primary macrophages, likely due to the significant upregulation of PARP enzymes (32). Thus, we tested the ability of IFN-β pretreatment to impede SARS-CoV-2 WT and ΔMac1 infection in Calu-3 cells. We found that adding increasing amounts of IFN-β to cells 18 h before infection reduced ΔMac1 replication to the same degree as WT virus in Calu-3 cells (Fig. 3*A*), indicating that SARS-CoV-2 ΔMac1 is not more sensitive to IFN-β than WT virus. We hypothesized that SARS-CoV-2 may be too sensitive to IFN-β to distinguish any difference in the replication of WT and ΔMac1 viruses. Therefore, we next used IFN-γ, which induces a smaller number of ISGs and has reduced antiviral activity against SARS-CoV-2 compared to IFN-β (42), but still induces the expression of PARP enzymes (*SI Appendix*, Fig. S4) (43). In contrast to results with IFN-β, pretreatment of cells with increasing concentrations of IFN-γ led to more robust inhibition of ΔMac1 than WT virus when cells were infected at an MOI of 0.1 and harvested at 48 hpi (Fig. 3*B*). The fold difference in replication between WT and ΔMac1 ranged from 3-fold with no IFN-γ, which is consistent with results in Fig. 2, to an ~20-fold reduction in replication of ΔMac1 compared to WT virus when cells were pretreated with 500 units of IFN-γ (Fig. 3*B*). To reduce the likelihood of unintended disruption of other domains in nsp3 with the deletion virus, we engineered two distinct point mutants into nsp3 in the SARS-CoV-2 BAC to determine if they were also sensitive to IFN-γ pretreatment. We created N1062A and D1044A viruses (Fig. 1*B*), which are orthologous to N1040A and D1022A mutant SARS-CoVs. Prior enzymatic analysis in other macrodomains has indicated that the N-A mutation largely ablates hydrolysis activity but maintains the ability to bind to ADP-ribose, though the affinity is reduced by twofold to threefold. Conversely, the D-A mutation largely abolishes binding activity but retains a significant amount of enzymatic activity (18, 44–46). Both viruses replicated at near WT levels in Calu-3 cells; however, only the N1062A mutant was more sensitive to IFN-γ pretreatment than WT virus (Fig. 3 *C* and *D*). These results indicate that Mac1 enzyme activity may be important for countering IFN-γ activity during a SARS-CoV-2 infection. In addition, a recent preprint also found that an N1062D mutation, which significantly reduced enzyme but not binding activity, was also more sensitive to IFN-γ pretreatment that WT virus (47). These results demonstrate that IFN-γ pretreatment of Calu-3 cells more effectively impedes the replication of SARS-CoV-2 Mac1 mutant viruses compared to WT virus, likely due to the loss of Mac1 ADP-ribosylhydrolase activity.

SARS-CoV-2 ΔMac1 Induces Increased IFN and Cytokine Responses in Cell Culture. Next, we tested SARS-CoV-2 ΔMac1 for its ability to induce IFNs and proinflammatory cytokines in cell culture, as has previously been shown for Mac1 mutants in SARS-CoV and MHV (18, 32). We found that in both Calu-3 and A549-ACE2 cells ΔMac1 infection induced greater levels of both IFN-I and IFN-III transcript levels and of ISGs such as ISG15

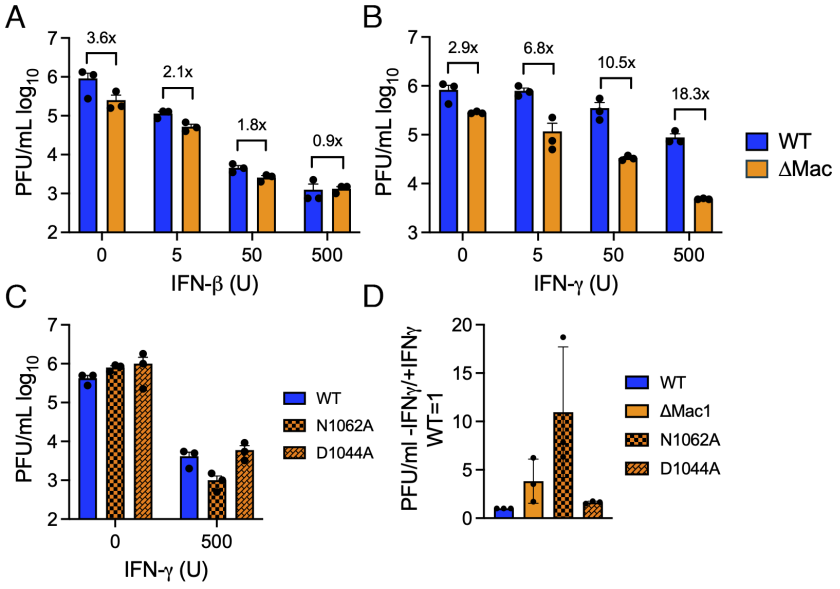

Fig. 3. IFN-γ, but not IFN-β, pretreatment enhances replication defect of ΔMac1 and Mac1 point mutant viruses in Calu-3 cells. Calu-3 cells were pretreated for 18 h with increasing concentrations (0, 5, 50, and 500 units) of IFN-β (*A*) and IFN-γ (*B*), then infected with either SARS-CoV-2 WT or ΔMac1 at an MOI of 0.1 PFU/cell. Cells were collected at 48 hpi, and titers were determined by the plaque assay. Fold differences between WT and ΔMac1 are indicated at each amount of IFN. The data shown are of one experiment representative of two (*A*) and three (*B*) independent experiments with $n = 3$ for each group. (*C*) Calu-3 cells were pretreated with 500 units of IFN-γ for 18 h and infected with SARS-CoV-2 WT, N1062A, and D1044A at an MOI of 0.1 PFU/cell. Cells were collected at 48 hpi, and titers were determined by the plaque assay. The data shown are of one experiment representative of three independent experiments with $n = 3$ for each group. (*D*) Fold-reduction of virus titer for each of the indicated viruses as compared to WT virus was determined. These data are the combined results of three independent experiments.

and CXCL-10 (Fig. 4 *A* and *B*). Protein levels of ISGs OAS3 and PARP14 were also significantly increased in ΔMac1-infected Calu-3 cells (Fig. 4 *C* and *D*). However, the increase in IFN/ISG transcript and protein levels, ~2- to 3-fold, is somewhat reduced compared to those prior results with SARS-CoV and MHV-JHM Mac1 mutant viruses (26, 32). This differences in IFN induction between WT and Mac1 deleted/mutant viruses between different CoVs could be due to alterations in the functions or abundance of other CoV-encoded IFN or IFN-signaling repressing proteins expressed by SARS-CoV-2.

SARS-CoV-2 ΔMac1 Is Highly Attenuated in K18-ACE2 Mice. We next tested the ability of SARS-CoV-2 WT, ΔMac1, and Mac1 point mutant viruses to cause disease in K18-ACE2 C57BL/6 mice, a lethal animal model of SARS-CoV-2 infection. Following intranasal inoculation of 2.5×10^4 PFU WT SARS-CoV-2, we observed 100% morbidity and mortality. In contrast, SARS-CoV-2 ΔMac1 infection did not cause any weight loss or lethality, indicating extreme attenuation (Fig. 5 *A* and *B*). We also tested N1062A and D1044A for the ability to cause severe disease. Both mutant viruses were attenuated, but not to the degree of ΔMac1 (Fig. 5 *C* and *D*), indicating that both loss of ADP-ribosylhydrolase and ADP-ribose binding activity contribute to the attenuation of ΔMac1 in mice. When analyzing the ΔMac1-infected lungs by hematoxylin and eosin (H & E) staining, we noted significantly higher levels of bronchointerstitial pneumonia, inflammation, and edema and fibrin in WT SARS-CoV-2-infected lungs compared to ΔMac1 virus–infected lungs (Fig. 5 *E* and *F*). We then compared the WT and ΔMac1 SARS-CoV-2 loads in infected lungs and found that by day 1 post infection, there was a significant reduction in viral titers (Fig. 5*G*) and viral genomic RNA (gRNA) (Fig. 5*H*) of ~1 log in the lungs of ΔMac1-infected mice compared to WT SARS-CoV-2-infected lungs. The difference in viral load between WT and ΔMac1 increased to 2.5 logs by day 3, and by day 7, ΔMac1 was effectively cleared from the lungs, while WT virus was still present at about 10^5 PFU in the lung (Fig. 5 *E* and *F*). In contrast, viral loads in the brain were very low until after day 3 post infection, though WT virus was present at low levels in most mice by day 7, whereas ΔMac1 titers were below the detection limit on all days tested. (*SI Appendix*, Fig. S5*A*). Further, there was no significant difference in brain pathology between WT and ΔMac1-infected mice at 7 dpi (*SI Appendix*, Fig. S5*B*), indicating that brain infection and pathology may not significantly contribute to the weight loss and mortality of WT infected mice; however, we cannot rule out mild to moderate effects of the brain infection to weight loss and mortality in WT infected mice.

SARS-CoV-2 ΔMac1 Induces a Robust Innate Immune Response in the Lungs of K18-ACE2 Mice. The rapid clearance of ΔMac1 in the lungs of infected mice and prior results with Mac1 SARS-CoV

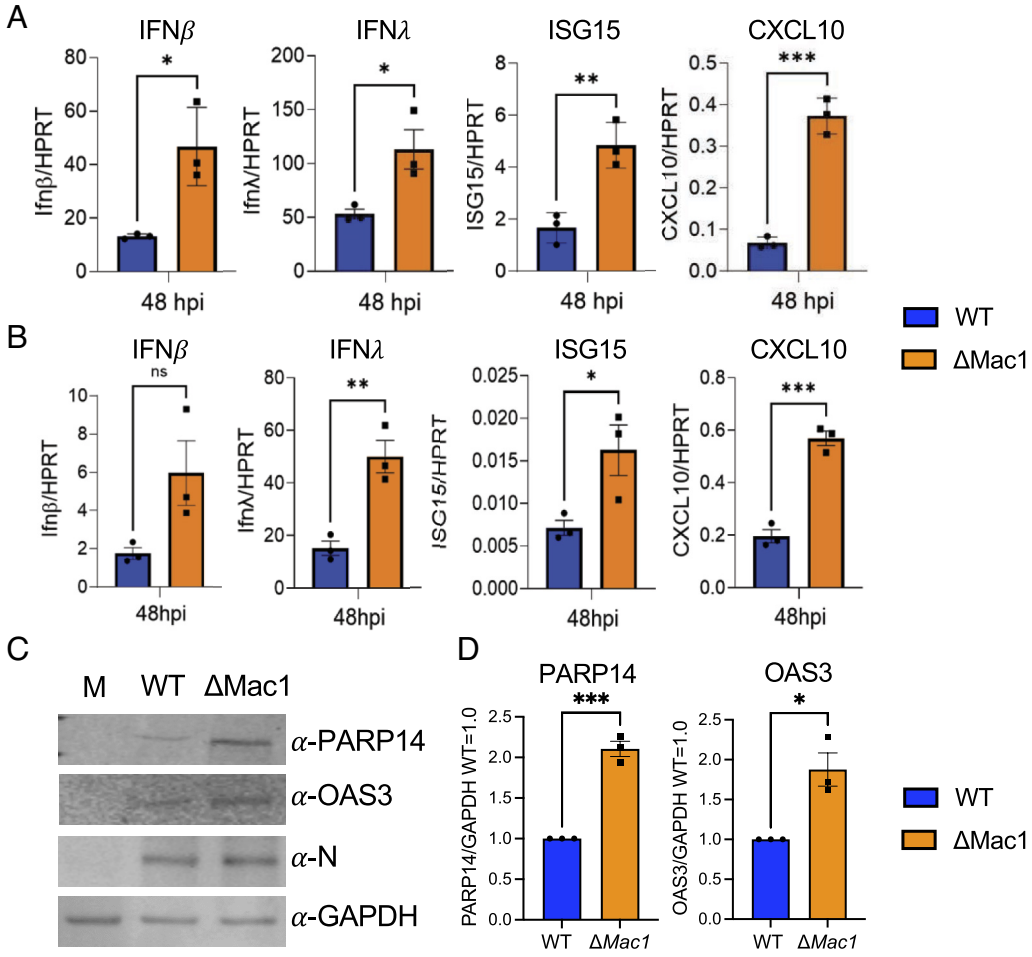

Fig. 4. ΔMac1 induces increased IFN-I, IFN-III, and cytokine responses compared to WT SARS-CoV-2 in cell culture. Calu-3 (*A*) and A549-ACE2 (*B*) cells were infected with SARS-CoV-2 WT and ΔMac1 at an MOI of 0.1 PFU/cell, and total RNA was collected 48 hpi. IFN-β, IFN-λ, ISG15, and CXCL10 levels were determined by qPCR using the ΔCt method with primers listed in *SI Appendix*, Table S2 and normalized to HPRT mRNA levels. The data show one experiment representative of three independent experiments with $n = 3$ for each experiment. (*C*) Calu-3 cells were infected as described above, and cell lysates were collected at 48 hpi and protein levels of PARP14 and OAS3 were determined by immunoblotting. The data show one experiment representative of three independent experiments. (*D*) Quantification of immunoblots shown in *C*. The data are the combined results of three independent experiments.

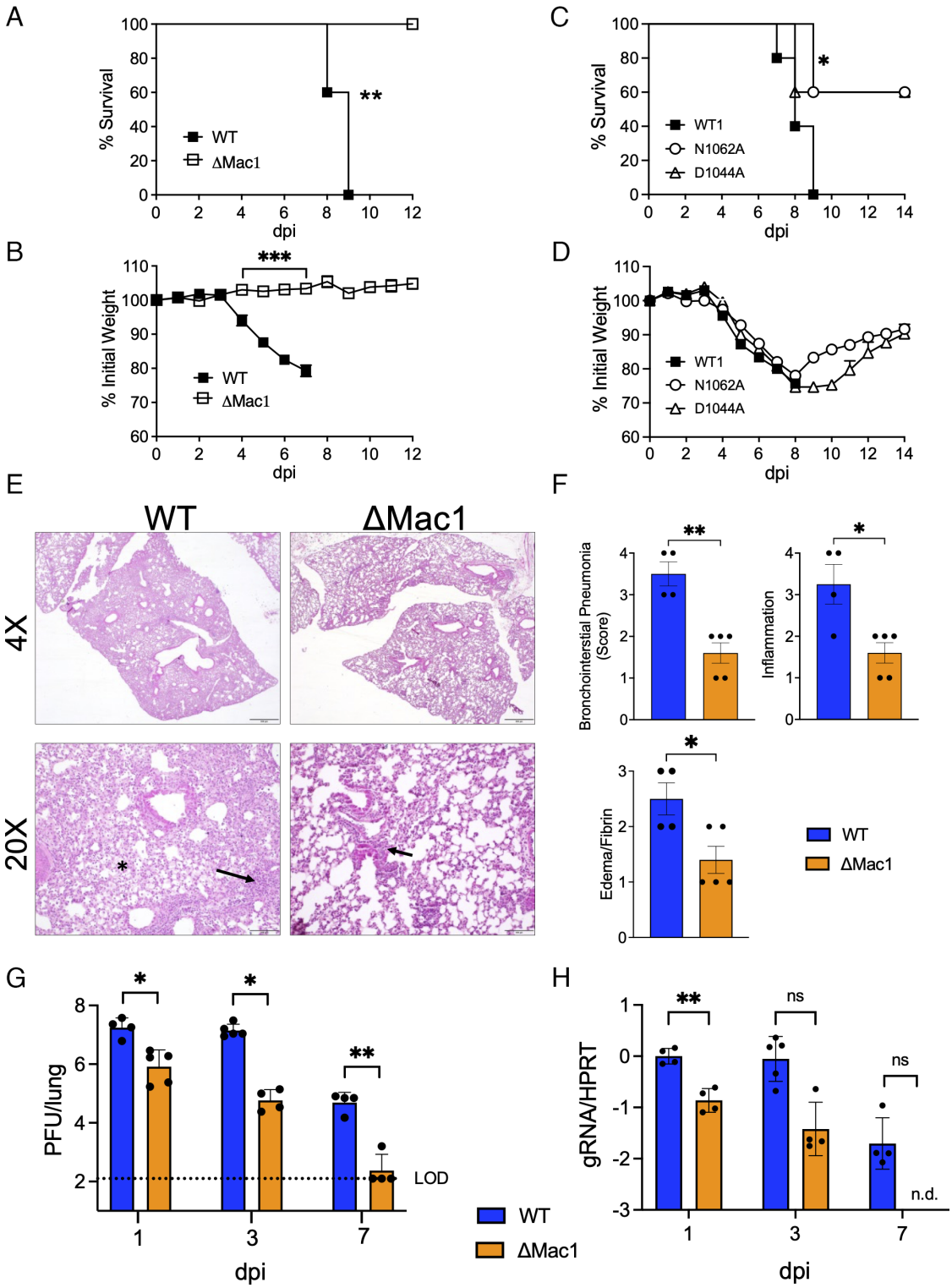

Fig. 5. ΔMac1 is highly attenuated in K18-ACE2 mice. (*A* and *B*) K18-ACE2 C57BL/6 mice were infected with 2.5 × 10^4 PFU of WT or ΔMac1 SARS-CoV-2 and survival (*A*) and weight loss (*B*) were measured over 12 d. (*C* and *D*) K18-ACE2 C57BL/6 mice were infected with 2.5 × 10^4 PFU of WT, N1062, and D1044A and survival (*C*) and weight loss (*D*) were measured over 14 d. (*A*–*D*) n = 5 for each group. (*E*) Photomicrographs (hematoxylin and eosin stain) of lungs from WT and ΔMac1-infected mice at 7 dpi demonstrating bronchointerstitial pneumonia (black arrow) and edema and fibrin (black asterisk). (*F*) Mice were scored for bronchointerstitial pneumonia, inflammation, and edema/fibrin deposition. (*G* and *H*) WT *n* = 4; ΔMac1 n = 5. (*G* and *H*) K18-ACE2 C57BL/6 mice were infected as described above and lung titers (*G*) and gRNA levels (*H*) were determined by the plaque assay and RT-qPCR with primers specific for nsp12 and normalized to HPRT, respectively. Results are from one experiment representative of two independent experiments with *n* = 4 to 10 mice per group.

mutant viruses (18) suggested that ΔMac1 would induce a strong innate immune response in mice. To test this possibility, we measured the transcripts of a small panel of IFNs and ISGs for their expression following infection of WT and ΔMac1 at 1 d post infection (Fig. 6*A*). IFN-β and IFN-λ were up-regulated by more than 10-fold in ΔMac1-infected lungs, while IFN-γ was not detected. We also observed a 2- to 3-fold increase in several ISGs, such as OAS, ISG15, CXCL10, IL-6, PARP12, and

PARP14. These results suggest that the attenuation of ΔMac1 virus could, at least in part, be due to a robust IFN response at the early stages of infection. To get a global view of all the transcriptional changes occurring in the absence of Mac1, we performed RNAseq of whole-lung samples collected on day 1 post infection (48). Differentially expressed genes were defined as having at least 1.5-fold increased expression in either WT or ΔMac1-infected lungs with an adjusted *P* value of <0.05. In total, we found that 645 genes were increased following infection with ΔMac1, and another 230 were increased following WT infection, including viral gRNA, for a total of 875 differentially regulated genes (Fig. 6*B*). Gene ontology analysis revealed that genes related to immunity, innate immunity, and antiviral defense were the pathways that were most significantly up-regulated in ΔMac1-infected lungs (Fig. 6*C*). In addition, genes in the categories of adaptive immunity, ubiquitin conjugation, inflammatory responses, peptide transport, cytolysis, and apoptosis were also significantly up-regulated in ΔMac1-infected lungs (Fig. 6*C*). We then looked at the individual expression of a panel of ISGs and found that most ISGs were increased between 2- and 4-fold in ΔMac1 when compared to WT virus infection, while IFN-β and IFN-λ were increased more than 10-fold (*SI Appendix*, Fig. S6). In total, we have found that Mac1 is required for SARS-CoV-2 to block the innate immune response during SARS-CoV-2 infection in mice.

SARS-CoV-2 ΔMac1 Infection Results in Reduced Myeloid Cell Accumulation in the Lungs. Next, we assessed the impact of WT and ΔMac1 virus infection on the recruitment of innate immune cells, specifically inflammatory monocytes and neutrophils, into the lung that might contribute to differential lung inflammation and disease severity. Inflammatory monocytes were found to contribute to disease severity in SARS-CoV and MERS-CoV infected mice by promoting the production of TNFα and increased

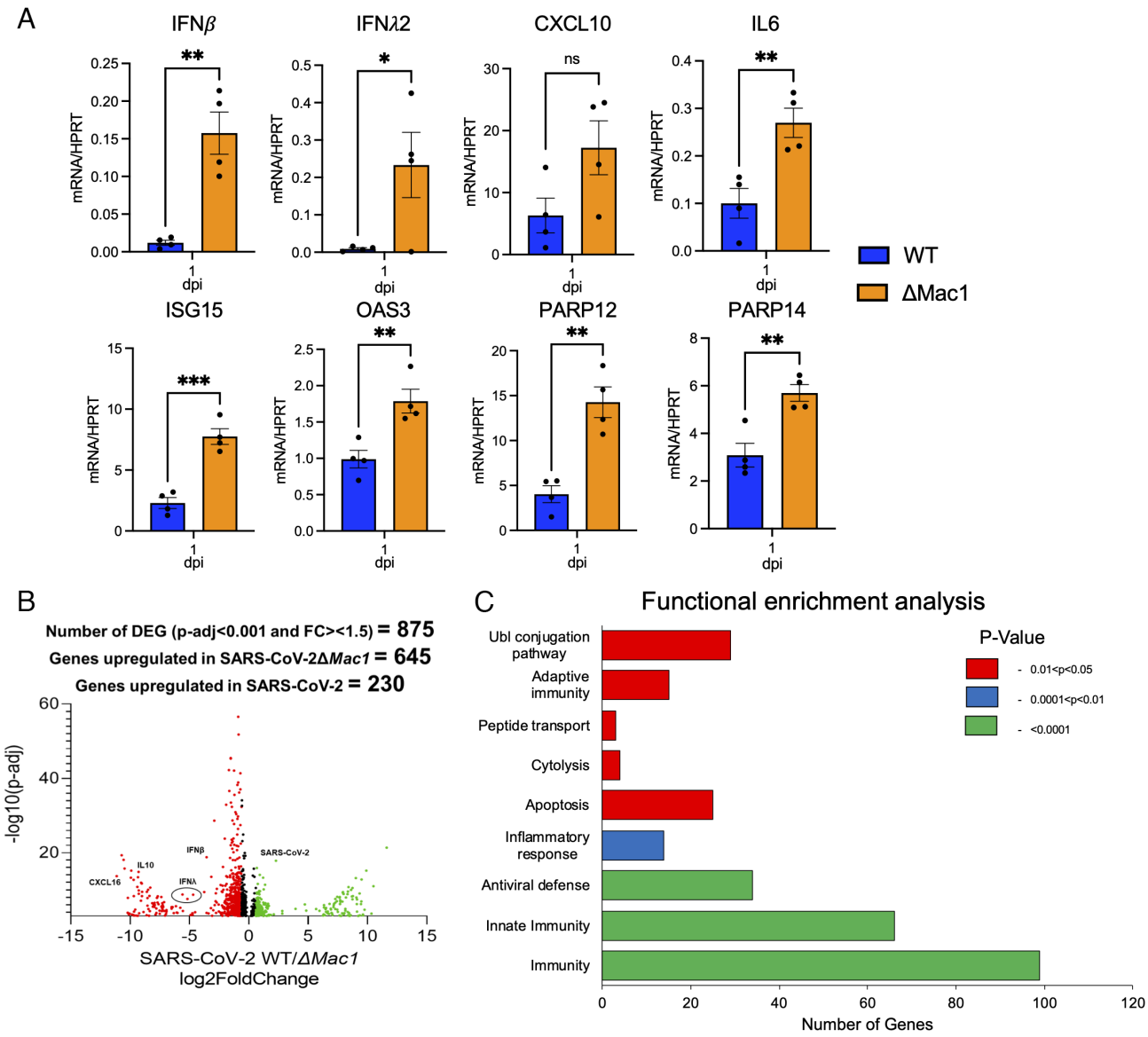

Fig. 6. ΔMac1 induces a robust innate immune response in the lungs following infection. (*A*) K18-ACE2 C57BL/6 mice were infected with 2.5 × 10^4 PFU of indicated viruses and lungs were harvested at 1 dpi and total RNA was isolated. The relative levels of indicated transcripts were determined by qPCR using the ΔCt method with primers listed in *SI Appendix*, Table S2 normalized to HPRT mRNA levels. The results are from one experiment representative of two independent experiments with *n* = 4 to 8 mice per group. (*B*–*C*) The total RNA from the samples in *A* was analyzed by RNAseq to determine the full transcriptome in the lung following infection. (*B*) Volcano plot indicating differentially expressed genes (DEGs) between WT and ΔMac1-infected mice. (*C*) Functional enrichment analysis of biological processes enriched in the transcriptome of mice infected with ΔMac1 performed using DAVID functional annotation tool.

T cell apoptosis (49, 50). Previously, IFN-I was shown to enhance inflammatory monocyte accumulation in the lung, though this was due to IFN-I production in the later stages of SARS-CoV replication (49). However, earlier exogenous addition of IFN-I reduced inflammatory monocyte infiltration following MERS-CoV infection was shown to reduce the number of inflammatory monocytes (50). Thus, we hypothesized that the early IFN-I and IFN-III induction by ΔMac1 would result in fewer infiltrating inflammatory immune cells. Following infection with ΔMac1, we observed a substantial reduction in both the percentage and total number of inflammatory monocytes at both 3 and 7 d after infection (Fig. 7*A*), which could also play a role in the attenuation of the disease severity. Neutrophils were slightly increased in percentage in ΔMac1-infected lungs on day 3 but had similar total numbers when compared to WT virus infection; however, by day 7 there was a significant reduction in the total number of neutrophils in ΔMac1-infected lungs (Fig. 7*B*).

Overall, our results indicate that the absence of Mac1 promotes a strong IFN response with a reduction in inflammatory cell types that may both play a role in reducing viral loads and preventing disease following infection.

Discussion

The COVID-19 pandemic caused by SARS-CoV-2 has fueled a new interest in the development of inhibitors targeting viral gene products that block viral replication and pathogenesis, to be used therapeutically to treat patients with COVID-19. This includes the $577 million-dollar Antiviral Drug Development Award (AVIDD) initiated by the NIH in 2021. Thus far, antivirals targeting the viral polymerase (nsp12) and protease (nsp5) have been approved for clinical use (4–6); however, a much larger anti-CoV drug portfolio is clearly needed to target SARS-CoV-2 and effectively respond to novel CoV outbreaks in the future. One of the CoV-encoded proteins that has received increased attention as a potential drug target is the conserved macrodomain, now called Mac1 (51). Multiple groups have initiated drug development programs targeting Mac1, all utilizing biochemical assays that can be used to screen for compounds that inhibit either Mac1-ADP-ribose binding or Mac1 ADP-ribosylhydrolase activity (34-41). Currently, the top Mac1 inhibitors identified to date have IC_{50} values in these biochemical assays ranging from ~0.5 to 10 μM. However, none of these compounds have been reported to inhibit virus replication or pathogenesis in cell culture or in mice. While the current body of literature indicates that Mac1 is important for the replication and pathogenesis of MHV and SARS-CoV in mice (18, 26, 31), no study has yet evaluated how Mac1 impacts the replication of SARS-CoV-2, which is critical for the ability to interpret inhibitor studies.

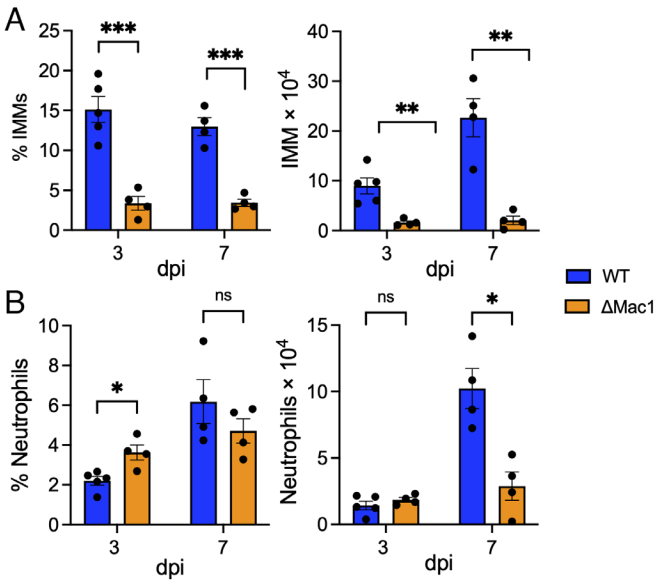

Fig. 7. ΔMac1 infection results in reduced inflammatory monocytes and neutrophils. (*A* and *B*) K18-ACE2 C57BL/6 mice were infected as described above, and lungs were harvested at the indicated days post infection, and the percentages and total numbers of infiltrating inflammatory monocytes (*A*) and neutrophils (*B*) were determined by flow cytometry. Data are derived from the results of one experiment representative of two independent experiments performed with *n* = 4 to 5 mice/group/experiment.

Prior results in our lab had indicated that Mac1 is critical for the replication of MHV-JHM, as at least two Mac1 mutant recombinant bacterial artificial chromosomes (BACs) failed to produce infectious virus (33). To confirm these results, we created a complete deletion of Mac1 in the MHV-JHM BAC and again found that we could not recover infectious virus (*SI Appendix*, Fig. S1 *A* and *B*). We hypothesized that perhaps a Mac1 deletion may be detrimental across CoVs, so we then created MERS-CoV and SARS-CoV-2 ΔMac1 recombinant BACs. Surprisingly, we were unable to recover infectious virus from the MERS-CoV ΔMac1 BAC but easily recovered infectious SARS-CoV-2 ΔMac1 (*SI Appendix*, Fig. S1 *A* and *B*). While we have not tested a Mac1 deletion in SARS-CoV, the near WT replication of the same G-V mutation in MHV that was unrecoverable indicates that Mac1 is likely nonessential for SARS-CoV as well (18). This near-absolute requirement for Mac1 in some CoV species but not in others was surprising, but not without precedent. For instance, a recombinant virus with an E protein deletion was viable with only a mild replication defect in SARS-CoV (52), but an E protein deletion in MERS-CoV was unrecoverable unless the virus was propagated on E protein–expressing cells (53). Nsp14 ExoN mutations are lethal in MERS-CoV and SARS-CoV-2 but are viable in MHV and SARS-CoV (54). Finally, MHV nsp15 mutant viruses grow very poorly in IFN-competent macrophages (55, 56), while similar mutations in MERS-CoV replicate normally in IFN-competent cells (57). In the cases of E protein and nsp15, the viruses that replicate normally in the absence of these proteins have additional accessory proteins that have overlapping or redundant functions. For instance, the 4a and 4b MERS-CoV proteins were found to have redundant functions with nsp15 in blocking the innate immune response to infection (57). We hypothesize that the Sarbecoviruses may have evolved unique accessory proteins or other domains in the nonstructural proteins that have redundant functions with Mac1 in promoting viral replication. One intriguing hypothesis is that one or both of the additional macrodomains in Sarbecoviruses (Mac2/Mac3) may functionally compensate for the loss of Mac1, even though they do not share the same biochemical functions. Efforts to identify proteins that can functionally compensate for Mac1 are ongoing. Regardless, we and others have found that Mac1 is critical for CoVs to replicate efficiently and cause disease in all animal models of infection that have been tested (Fig. 5) (18, 26, 31).

Mac1 is only a small domain within nsp3, but there is the potential for a complete deletion to impact other domains within nsp3, including PLpro. Previously, it was shown in MHV that PLP2 can interact with Mac1, and mutations in Mac1 outside of the ADP-ribose binding pocket were found to have a temperature-dependent phenotype (58). However, PLpro is essential for polyprotein processing and virus replication, but here, we found that there was no defect in nsp3 staining or in the replication of ΔMac1 in Vero E6 and A549 cells, and only a modest defect in

Calu-3 cells. In addition, the phenotypes we observed, including increased IFN production, have previously been observed following Mac1 point mutant virus infection with SARS-CoV and MHV (18, 32). We have also demonstrated that these phenotypes in MHV can be reversed with PARP inhibitors or siRNAs (32). Given these results, along with modularity of the various domains of nsp3, it is unlikely that the complete deletion of Mac1 had a significant effect on the functions of its various domains or the overall structure of nsp3. However, we cannot rule out modest impacts on other nsp3 domains without the ability to complement virus replication with Mac1 expression outside the context of nsp3.

Despite the lack of a large replication defect of ΔMac1 under normal growth conditions, we found that ΔMac1 had a >1 log defect in IFN-γ, but not IFN-β-treated Calu-3 cells (Fig. 5). IFN-γ induces a small number of ISGs compared to IFN-β, but it does induce PARP expression (*SI Appendix*, Fig. S4) (43). We hypothesize that while the PARP enzymes that inhibit Mac1 mutant SARS-CoV-2 are up-regulated by both types of IFN, other more potent anti-SARS-CoV-2 ISGs are only up-regulated by IFN-β, or at least up-regulated to a much higher level by IFN-β. We further hypothesize that IFN-I ISGs might limit viral entry, mitigating the effect of PARP enzymes to specifically target the Mac1 mutant virus during later stages of the viral lifecycle. It will be of interest to identify the specific PARPs or other ISGs that inhibit ΔMac1 following IFN-γ treatment. The ability to specifically reduce ΔMac1 replication with IFN-γ could have important implications for Mac1 inhibitor testing. Replication assays could be developed to assess the ability of the Mac1 inhibitors to reduce virus replication in the absence and presence of IFN-γ to show that the inhibitors are indeed specifically targeting Mac1. It may also be of interest to test the replication of ΔMac1 under conditions of cell stress, such as ER stress or following activation of stress granules, as PARP activity is known to be increased under stress conditions (59, 60).

One puzzling question is why there is a substantial difference in the replication of ΔMac1 in cell culture, where we saw only a 2- to 3-fold reduction, compared to its replication in mice, where there was nearly a 1-log difference in viral loads at 1 dpi, and a >2-log difference at 3 dpi compared to WT virus. One hypothesis is that IFN-γ produced in the lung by NK cells at early time-points (1 and 3 dpi) and T cells during later stages (after 5 dpi) can dramatically reduce ΔMac1 replication due to its increased sensitivity to IFN-γ. On the other hand, it could be that despite similar sensitivity of both viruses to IFN-I and IFN-III, increased amounts of these antiviral cytokines produced in ΔMac1-infected lungs are able to greatly suppress ΔMac1 replication. Similar to SARS-CoV N1040A, we found that SARS-CoV-2 ΔMac1 induces an early robust innate immune response in mice (Figs. 4 and 6), further confirming that Mac1 is one of the many potent IFN repressing proteins expressed by CoVs. This innate immune response occurred within 1 d of infection and likely before peak replication of the virus. Whole-lung RNAseq data identified over 100 genes involved in immunity to virus infection that are triggered following ΔMac1 infection, demonstrating the breadth of the immune response initiated by ΔMac1 (Fig. 6 *B*–*D*). We have previously shown that the MHV-JHM Mac1 mutant virus, N1347A, causes increased lethality and weight loss in IFNAR knockout mice (IFN-I deficient) and that providing exogenous IFN-I or IFN-III prior to peak viral replication is highly protective in multiple animal models of CoV infection (32, 49, 50). COVID-19 patients with mutations in IFN-related genes or that produce antibodies that target IFN-I have worse outcomes than the general population, demonstrating the importance of IFN-I in protection from severe COVID-19 (61–63). These results indicate that the early production of IFN-I and IFN-III likely acts to limit the replication and pathogenesis of ΔMac1, though we cannot rule out a contribution from IFN-γ. Future experiments should be designed to test these two hypotheses. Furthermore, it remains unclear how an early IFN response from a virus contributes to the protection of mice, and potentially humans, from disease. Some important questions include the following: How is the IFN induced? Is it through MDA5, RIG-I, or other sensors? Which cell type is the major source of IFN-I and IFN-III? Are both IFN-I and IFN-III important for protection, or is one of them sufficient? Do they alter the functions of innate immune cells, such as macrophages, and finally, how do these IFNs shape the adaptive immune response? The answers to these and other questions could have important implications for developing vaccines or therapeutics that might stimulate better and longer-lasting immunity and reduce incidence of SARS-CoV-2 spread and disease in vulnerable populations.

Methods

Cell Culture and Reagents. Vero E6, Huh-7, Baby Hamster Kidney cells expressing the mouse virus receptor CEACAM1 (BHK-MVR) (gifts from Stanley Perlman, University of Iowa), and A549-ACE2 cells (a gift from Susan Weiss, University of Pennsylvania), were grown in Dulbecco's modified Eagle medium (DMEM) supplemented with 10% fetal bovine serum (FBS). Calu-3 cells (ATCC) were grown in MEM supplemented with 20% FBS. Human IFN-β and IFN-γ were purchased from R&D Systems. Cells were transfected with either Polyjet (Amgen) or Lipofectamine 3,000 (Fisher Scientific) per the instructions of the manufacturers.

Primary human bronchial epithelial cells (HBECs) were harvested from healthy donors whose lungs were rejected for transplant and with unknown airway disease. Passage 0 cells were expanded in PneumaCult™-Ex Plus Medium (STEMCELL Technologies), supplemented with gentamicin (ThermoFisher Scientific) and amphotericin B (ThermoFisher Scientific). When the cells reached confluency, they were passaged and expanded a second time in bronchial epithelial cell growth medium before being seeded on translucent Thincert (Greiner), at a density of 2×10^5 cells in air-liquid interface media, as previously described (64) (See *SI Appendix*, *Supplemental Methods* for further details).

Mice. Pathogen-free K18-ACE2 C57BL/6 mice were purchased from Jackson Laboratories. Mice were bred and maintained in the animal resources facility at the Oklahoma State University. Animal studies were approved by the Oklahoma State University Institutional Animal Care and Use Committee and met stipulations of the Guide for the Care and Use of Laboratory Animals.

Generation of Recombinant pBAC-SARS-CoV-2, pBAC-MERS-CoV, and pBAC-JHMV Constructs. All recombinant pBAC constructs were created using Red recombination (65, 66) with several previously described CoV BACs. These include the WT-SARS-CoV-2 BAC based off the Wuhan-Hu-1 isolate provided by Sonia Zuñiga, Li Wang, Isabel Sola and Luis Enjuanes (CNB-CSIC, Madrid, Spain) (67), a MERS-CoV BAC based off of the EMC isolate (53), and an MHV BAC based off of the JHMV isolate (26). See *SI Appendix*, *Supplemental Methods* for additional details.

Reconstitution of Recombinant pBAC-SARS-CoV-2-Derived Virus. All work with SARS-CoV-2 and MERS-CoV was conducted in either the University of Kansas or the Oklahoma State University EHS-approved BSL-3 facilities. To generate SARS-CoV-2 or MERS-CoV, approximately 5×10^5 Huh-7 cells were transfected with 2 μg of purified BAC DNA using Lipofectamine 3,000 (Fisher Scientific) as a transfection reagent. SARS-CoV-2 generated from these transfections (p0) was then passaged in Vero E6 cells to generate viral stocks (p1). All p1 stocks were again sequenced by Sanger sequencing to confirm that they retained the correct Mac1 deletion and to ensure that the furin cleavage site had not been lost (for primers see *SI Appendix*, Table S2). Furthermore, two independently recovered isolates of ΔMac1 had their genomes fully sequenced along with WT virus which confirmed that there were no second-site mutations in the viral stocks (SeqCenter) (68, 69). To generate MHV-JHM and MERS-CoV, approximately 5×10^5 BHK-MVR cells were transfected with 1 μg of purified BAC DNA using PolyJet™ Transfection Reagent (SignaGen). In the case of MHV-JHM, an additional 1 μg of N protein–expressing plasmid was cotransfected with genomic BAC DNA.

Virus Infection. Vero-E6, A549-ACE2, or Calu-3 cells were infected at the indicated MOIs. For Calu-3 cells, trypsin-TPCK (1 μg/mL) was added to the medium at the time of infection. All infections included a 1-h adsorption phase, except for Calu-3 cells where the adsorption phase was increased to 2 h. Infected cells and supernatants were collected at indicated time points and titers were determined on Vero E6 cells. For IFN pretreatment experiments, human IFN-β and IFN-γ were added to Calu-3 cells 18 to 20 h prior to infection and were maintained in the culture media throughout the infection. For animal infections, 12 to 16-wk-old K18-ACE2 C57BL/6 female mice were lightly anesthetized using isoflurane and were intranasally infected with 2.5×10^4 PFU in 50 μL DMEM. To obtain tissue for virus titers, mice were killed on different days post challenge, lungs or brains were removed and homogenized in phosphate buffered saline (PBS), and titers were determined on Vero E6 cells.

Immunoblotting. Total cell extracts were lysed in sample buffer containing SDS, protease and phosphatase inhibitors (Roche), β-mercaptoethanol, and a universal nuclease (Fisher Scientific). Proteins were resolved on an SDS polyacrylamide gel, transferred to a polyvinylidene difluoride (PVDF) membrane, hybridized with a primary antibody, reacted with an infrared (IR) dye-conjugated secondary antibody, visualized using a Li-COR Odyssey Imager (Li-COR), and analyzed using Image Studio software. Primary antibodies used for immunoblotting included anti-SARS-CoV-2 N (SinoBiological 40143-R001, 1:5,000), anti-OAS3 (Cell Signaling 41440, 1:250), anti-PARP14 (Santa Cruz Biotechnology SC-377150, 1:100), and anti-GAPDH (Millipore-Sigma G8795, 1:5,000) antibodies. Secondary IR antibodies were purchased from Li-COR.

Confocal Immunofluorescence. Calu-3 cells were cultured with approximately 1.4×10^5 cells per well in 8-well, removable chamber slides (ibidi 80841) and infected with SARS-CoV-2 at an MOI of 1 PFU/cell. At 24 hpi, monolayers were fixed for 20 min with ice-cold methanol and then 10 min with 2% paraformaldehyde in HBSS + 0.01% Sucrose (HBSS/Su). Permeabilization with 0.1% Saponin in HBSS/Su was then performed, followed by overnight blocking at 4 °C using 3% goat serum in HBSS/Su + Saponin. Primary antibody incubation was conducted for 3 h at room temperature (1:2,000 α-N protein, Sino Biological 40143-R001; 1:500 α-nsp3, abcam ab283958) followed by a 1 h, room temperature secondary antibody incubation (1:200 AlexaFluor 555 Goat α-rabbit, Invitrogen A32732). Nuclear stain with 300 nM DAPI was performed at room temperature for 30 min followed by mounting in Vectashield Vibrance Mounting Medium (Vector Labs H-1700) and storage at 4 °C. Images were acquired using an Olympus FV1000 laser-scanning confocal microscope equipped with Fluoview software. Images were z-projected using maximum intensity.

Semiquantitative PCR Analysis. BAC DNA or infection-derived cDNA was PCR amplified by primers that bind outside of the Mac1 coding sequence. PCR products were analyzed by gel electrophoresis using a LICOR M imager and bands were quantified using Image Studio software, and the relative intensity of each band was determined by adding the overall intensity of both bands together and then diving the intensity of each individual band by the total intensity.

Real-Time (RT-qPCR) Analysis. RNA was isolated from cells using Trizol (Invitrogen). Lungs from K18-ACE2 C57BL/6 mice infected with virus were collected at indicated time points and were homogenized in Trizol (Invitrogen), and RNA was isolated using the manufacturer's instructions. cDNA was prepared using MMLV-reverse transcriptase per the manufacturer's instructions (ThermoFisher Scientific). qPCR was performed using PowerUp SYBR green master mix (Applied Biosystems) and primers listed in *SI Appendix*, Table S3. Cycle threshold values were normalized to hypoxanthine phosphoribosyltransferase (HPRT) levels by using the ΔCt method.

RNAseq. RNA was isolated from K18-ACE2 mice as described above. Library preparation was performed by the University of Kansas Genome Sequencing core facility, using the NEB Next RNA Library kit (NEB) with indexing. RNAseq was performed using an Illumina NextSeq2000 high-output system with paired-end reads of 50 bp each. DESeq2 was used to identify DEGs between the SARS-CoV-2 WT and ΔMac1-infected samples using simply "treatment" as a factor. DEGs were identified based on the false-discovery rate corrected *P*-value (P_{ADJ}) and $\log_2$-fold-change of ($\log_2$FC) between the samples. Genes were considered up-regulated in a SARS-CoV-2-infected sample if $P_{ADJ} < 0.05$ and $\log_2FC > 0.6$, which is nearly equivalent to a 1.5-fold increase. Similarly, genes were considered down-regulated if $P_{ADJ} < 0.05$ and $\log_2FC < -0.6$, or a 1.5-fold decrease. For additional RNAseq methods, see Supplemental Methods. DEGs were subjected to gene ontology analysis using the Database for Annotation, Visualization and Integrated Discovery (DAVID: https://david.ncifcrf.gov/). Gene lists were analyzed for biological processes that were significantly enriched with $P < 0.05$ and displayed as a clustered bar graph.

Lung Cell Preparation and Flow Cytometry. For phenotypic analyses of lung infiltrating immune cells, PBS-perfused lungs were treated with collagenase-D and DNAse1 for 30 min at room temperature, followed by homogenization of lung pieces using a 3 mL syringe plunger flang/thumb rest. Isolated single-cell suspension was surface immunolabeled for neutrophil ($CD45^+$ $CD11b^+$ $Ly6G^{hi}$) and inflammatory monocyte ($CD45^+$ $CD11b^+$ $Ly6c^{hi}$) markers by flow cytometry. For cell surface staining, lung cells were labeled with the following fluorochrome-conjugated monoclonal antibodies: PECy7 α-CD45 (clone: 30-F11); FITC α-Ly6G (clone: 1A8); PE/PerCp-Cy5.5 α-Ly6C (clone: HK1.4); V450 α-CD11b (clone: M1/70); APC α-F4/80 (clone: BM8) (all procured from BioLegend). A detailed cell surface and intracellular immunolabeling protocol for flow cytometry studies is described in our recent publication (70). All fluorochrome-conjugated antibodies were used at a final concentration of 1:200 (antibody: FACS buffer), except for FITC-labeled antibodies used at 1:100 concentration.

Histopathology. The lung lobes were perfused and placed in 10% formalin. Brain samples were fixed in 10% formalin. The lung lobes and brain were then processed for (H & E). The lung lesions were blindly scored by an American College of Veterinary Pathology Board-certified pathologist. The lesions were scored on a scale of 0 to 10% (score 1), 10 to 40% (score 2), 40 to 70% (score 3), and >70% (score 4), and cumulative scores were obtained for each mouse. The lesions scored were bronchointerstitial pneumonia, peribronchial inflammation, edema/fibrin, necrosis, and perivascular inflammation.

Statistics. A Student's *t* test was used to analyze differences in mean values between groups. All results are expressed as means ± SEM. Differences in survival were calculated using a Kaplan–Meier log-rank test. *P* values of ≤0.05 were considered statistically significant (*$P \le 0.05$; **$P \le 0.01$; ***$P \le 0.001$; ****$P \le 0.0001$; n.s., not significant).

Data, Materials, and Software Availability. All the RNAseq reads data are deposited in NCBI under the BioProject ID PRJNA928501 (48) and BioSample ID SAMN32942656 (71) and SAMN32942675 (72) and will be made public upon publication or August 31st 2023, whichever comes first. All study data are included in the article and/or supporting information.

ACKNOWLEDGMENTS. We thank members of the Davido laboratory at KU for valuable discussion, Stanley Perlman and Susan Weiss for reagents, and Brian Ackley for assistance with confocal microscopy. Bioinformatic consultation was provided by the KU Center for Genomics. Research reported in this publication was made possible in part by the services of the KU Genome Sequencing Core which is supported by the NIH under award number P30GM145499. We thank the Life Alliance Organ Recovery Agency from the University of Miami, Miami, FL, LifeCenter Northwest from Bellevue, Washington, Nevada Donor Network from Las Vegas, NV, and Midwest Transplant Network from Kansas City, KS, for providing the lungs. NIH grant P20GM103648 (R.C.) NIH grant 2P01AI060699 (L.E.) NIH grant P20GM113117 (A.R.F.) NIH grant K22AI134993 (A.R.F.) NIH grant R35GM138029 (A.R.F.) NIH grant R01HL139365 (M.S.) NIH grant R01HL133240 (M.S.) NIH grant R01HL157942 (M.S.) Cystic Fibrosis Foundation grant SALATH18I0 (M.S.) NSF grant 2135167 (R.L.U.) University of Kansas General Research Fund and Start-up funds (A.R.F.) NIH Graduate Training at the Biology-Chemistry Interface grant T32GM132061 (C.M.K.) University of Kansas College of Liberal Arts and Sciences Graduate Research Fellowship (C.M.K.) Government of Spain (PID2019-107001RB-I00 AEI/FEDER, UE) (L.E.) European Commission (H2020-SC1-2019, ISOLDA Project no. 848166-2) (L.E.).

Author affiliations: [a]Department of Molecular Biosciences, University of Kansas, Lawrence, KS 66047; [b]Department of Veterinary Pathobiology, Oklahoma State University, Stillwater, OK 74078; [c]Department of Internal Medicine, University of Kansas Medical Center, Kansas City, KS 66160; and [d]Department of Molecular and Cell Biology, National Center of Biotechnology, Madrid 28049, Spain

1. Y. Wang, M. Grunewald, S. Perlman, Coronaviruses: An updated overview of their replication and pathogenesis. *Methods Mol. Biol.* **2203**, 1–29 (2020).
2. D. Blanco-Melo *et al.*, Imbalanced host response to SARS-CoV-2 drives development of COVID-19. *Cell* **181**, 1036–1045.e1039 (2020).
3. E. P. K. Parker *et al.*, Response to additional COVID-19 vaccine doses in people who are immunocompromised: A rapid review. *Lancet Glob. Health* **10**, e326–e328 (2022).
4. J. H. Beigel, K. M. Tomashek, L. E. Dodd, Remdesivir for the treatment of covid-19 - preliminary report. *N. Engl. J. Med.* **383**, 994 (2020).
5. A. Wahl *et al.*, SARS-CoV-2 infection is effectively treated and prevented by EIDD-2801. *Nature* **591**, 451–457 (2021).
6. I. Gentile *et al.*, Nirmatrelvir/ritonavir and molnupiravir in the treatment of mild/moderate COVID-19: Results of a real-life study. *Vaccines (Basel)* **10**, 1731 (2022).
7. A. Chatterjee *et al.*, Nuclear magnetic resonance structure shows that the severe acute respiratory syndrome coronavirus-unique domain contains a macrodomain fold. *J. Virol.* **83**, 1823–1836 (2009).
8. M. A. Johnson, A. Chatterjee, B. W. Neuman, K. Wuthrich, SARS coronavirus unique domain: Three-domain molecular architecture in solution and RNA binding. *J. Mol. Biol.* **400**, 724–742 (2010).
9. Y. Kusov, J. Tan, E. Alvarez, L. Enjuanes, R. Hilgenfeld, A G-quadruplex-binding macrodomain within the "SARS-unique domain" is essential for the activity of the SARS-coronavirus replication-transcription complex. *Virology* **484**, 313–322 (2015).
10. S. Srinivasan *et al.*, Structural genomics of SARS-CoV-2 indicates evolutionary conserved functional regions of viral proteins. *Viruses* **12**, 360 (2020).
11. J. Tan *et al.*, The "SARS-unique domain" (SUD) of SARS coronavirus is an oligo(G)-binding protein. *Biochem. Biophys. Res. Commun.* **364**, 877–882 (2007).
12. J. Tan *et al.*, The SARS-unique domain (SUD) of SARS coronavirus contains two macrodomains that bind G-quadruplexes. *PLoS Pathog.* **5**, e1000428 (2009).
13. G. I. Makrynitsa *et al.*, Conformational plasticity of the VEEV macro domain is important for binding of ADP-ribose. *J. Struct. Biol.* **206**, 119–127 (2019).
14. H. Malet *et al.*, The crystal structures of Chikungunya and Venezuelan equine encephalitis virus nsP3 macro domains define a conserved adenosine binding pocket. *J. Virol.* **83**, 6534–6545 (2009).
15. Y. M. O. Alhammad *et al.*, The SARS-CoV-2 conserved macrodomain is a mono-ADP-ribosylhydrolase. *J. Virol.* **95**, e01969-20 (2021).
16. M. P. Egloff *et al.*, Structural and functional basis for ADP-ribose and poly(ADP-ribose) binding by viral macro domains. *J. Virol.* **80**, 8493–8502 (2006).
17. L. Eckei *et al.*, The conserved macrodomains of the non-structural proteins of Chikungunya virus and other pathogenic positive strand RNA viruses function as mono-ADP-ribosylhydrolases. *Sci. Rep.* **7**, 41746 (2017).
18. A. R. Fehr *et al.*, The conserved coronavirus macrodomain promotes virulence and suppresses the innate immune response during severe acute respiratory syndrome coronavirus infection. *mBio* **7**, e01721-16 (2016).
19. C. Li *et al.*, Viral macro domains reverse protein ADP-ribosylation. *J. Virol.* **90**, 8478–8486 (2016).
20. J. G. M. Rack *et al.*, Viral macrodomains: A structural and evolutionary assessment of the pharmacological potential. *Open. Biol.* **10**, 200237 (2020).
21. B. Luscher *et al.*, ADP-ribosyltransferases, an update on function and nomenclature. *FEBS J.* **289**, 7399–7410 (2021), 10.1111/febs.16142.
22. G. Caprara *et al.*, PARP14 controls the nuclear accumulation of a subset of type I IFN-inducible proteins. *J. Immunol.* **200**, 2439–2454 (2018).
23. A. R. Fehr *et al.*, The impact of PARPs and ADP-ribosylation on inflammation and host-pathogen interactions. *Genes Dev.* **34**, 341–359 (2020).
24. L. Li *et al.*, PARP12 suppresses Zika virus infection through PARP-dependent degradation of NS1 and NS3 viral proteins. *Sci. Signal.* **11**, eaas9332 (2018).
25. S. Parthasarathy, A. R. Fehr, PARP14: A key ADP-ribosylating protein in host-virus interactions? *PLoS Pathog.* **18**, e1010535 (2022).
26. A. R. Fehr *et al.*, The nsp3 macrodomain promotes virulence in mice with coronavirus-induced encephalitis. *J. Virol.* **89**, 1523–1536 (2015).
27. G. Jankevicius *et al.*, A family of macrodomain proteins reverses cellular mono-ADP-ribosylation. *Nat. Struct. Mol. Biol.* **20**, 508–514 (2013).
28. A. Putics, W. Filipowicz, J. Hall, A. E. Gorbalenya, J. Ziebuhr, ADP-ribose-1"-monophosphatase: A conserved coronavirus enzyme that is dispensable for viral replication in tissue culture. *J. Virol.* **79**, 12721–12731 (2005).
29. L. C. Russo *et al.*, The SARS-CoV-2 Nsp3 macrodomain reverses PARP9/DTX3L-dependent ADP-ribosylation induced by interferon signaling. *J. Biol. Chem.* **297**, 101041 (2021).
30. T. Kuri *et al.*, The ADP-ribose-1''-monophosphatase domains of severe acute respiratory syndrome coronavirus and human coronavirus 229E mediate resistance to antiviral interferon responses. *J. Gen. Virol.* **92**, 1899–1905 (2011).
31. K. K. Eriksson, L. Cervantes-Barragan, B. Ludewig, V. Thiel, Mouse hepatitis virus liver pathology is dependent on ADP-ribose-1''-phosphatase, a viral function conserved in the alpha-like supergroup. *J. Virol.* **82**, 12325–12334 (2008).
32. M. E. Grunewald *et al.*, The coronavirus macrodomain is required to prevent PARP-mediated inhibition of virus replication and enhancement of IFN expression. *PLoS Pathog.* **15**, e1007756 (2019).
33. L. S. Voth *et al.*, Unique mutations in the murine hepatitis virus macrodomain differentially attenuate virus replication, indicating multiple roles for the macrodomain in coronavirus replication. *J. Virol.* **95**, e0076621 (2021).
34. M. Dasovich *et al.*, High-throughput activity assay for screening inhibitors of the SARS-CoV-2 Mac1 macrodomain. *ACS Chem. Biol.* **17**, 17–23 (2022).
35. M. Schuller *et al.*, Fragment binding to the Nsp3 macrodomain of SARS-CoV-2 identified through crystallographic screening and computational docking. *Sci. Adv.* **7**, eabf8711 (2021).
36. L. M. Sherrill *et al.*, Design, synthesis and evaluation of inhibitors of the SARS-CoV-2 nsp3 macrodomain. *Bioorg. Med. Chem.* **67**, 116788 (2022).
37. S. T. Sowa *et al.*, A molecular toolbox for ADP-ribosyl binding proteins. *Cell Rep. Methods* **1**, 100121 (2021), 10.1016/j.crmeth.2021.100121.
38. R. S. Virdi *et al.*, Discovery of drug-like ligands for the Mac1 domain of SARS-CoV-2 Nsp3. *SLAS Discov.* **25**, 1162–1170 (2020).
39. G. J. Correy *et al.*, The mechanisms of catalysis and ligand binding for the SARS-CoV-2 NSP3 macrodomain from neutron and x-ray diffraction at room temperature. *Sci. Adv.* **8**, eabo5083 (2022).
40. A. Roy *et al.*, Discovery of compounds that inhibit SARS-CoV-2 Mac1-ADP-ribose binding by high-throughput screening. *Antiviral. Res.* **203**, 105344 (2022).
41. S. Gahbauer *et al.*, Iterative computational design and crystallographic screening identifies potent inhibitors targeting the Nsp3 macrodomain of SARS-CoV-2. *Proc. Natl. Acad. Sci. U.S.A.* **120**, e2212931120 (2023).
42. I. Busnadiego *et al.*, Antiviral activity of Type I, II, and III interferons counterbalances ACE2 inducibility and restricts SARS-CoV-2. *mBio* **11**, e01928-20 (2020).
43. S. Y. Liu, D. J. Sanchez, R. Aliyari, S. Lu, G. Cheng, Systematic identification of type I and type II interferon-induced antiviral factors. *Proc. Natl. Acad. Sci. U.S.A.* **109**, 4239–4244 (2012).
44. G. I. Karras *et al.*, The macro domain is an ADP-ribose binding module. *EMBO J.* **24**, 1911–1920 (2005).
45. R. L. McPherson *et al.*, ADP-ribosylhydrolase activity of Chikungunya virus macrodomain is critical for virus replication and virulence. *Proc. Natl. Acad. Sci. U.S.A.* **114**, 1666–1671 (2017).
46. R. Abraham *et al.*, Both ADP-ribosyl-binding and hydrolase activities of the alphavirus nsP3 macrodomain affect neurovirulence in mice. *mBio* **11**, e03253-19 (2020).
47. T. Y. Taha *et al.*, A single inactivating amino acid change in the SARS-CoV-2 NSP3 Mac1 domain attenuates viral replication and pathogenesis in vivo. bioRxiv[Preprint] (2023). 10.1101/2023.04.18.537104 (Accessed 24 April 2023).
48. S. Parthasarathy, R. Ghimire, A. Fehr, R. Channappanavar, RNAseq of K18-ACE2 C57BL6 mice lungs infected with SARS-CoV-2 WT strain vs its corresponding Mac1 deletion mutant. Sequence Read Archive (SRA) NCBI. https://www.ncbi.nlm.nih.gov/bioproject/PRJNA928501. Deposited 26 January 2023.
49. R. Channappanavar *et al.*, Dysregulated type I interferon and inflammatory monocyte-macrophage responses cause lethal pneumonia in SARS-CoV-infected mice. *Cell Host Microbe* **19**, 181–193 (2016).
50. R. Channappanavar *et al.*, IFN-I response timing relative to virus replication determines MERS coronavirus infection outcomes. *J. Clin. Invest.* **129**, 3625–3639 (2019).
51. A. K. L. Leung, D. E. Griffin, J. Bosch, A. R. Fehr, The conserved macrodomain is a potential therapeutic target for coronaviruses and alphaviruses. *Pathogens* **11**, 94 (2022).
52. M. L. DeDiego *et al.*, A severe acute respiratory syndrome coronavirus that lacks the E gene is attenuated in vitro and in vivo. *J. Virol.* **81**, 1701–1713 (2007).
53. F. Almazan *et al.*, Engineering a replication-competent, propagation-defective Middle East respiratory syndrome coronavirus as a vaccine candidate. *mBio* **4**, e00650–00613 (2013).
54. N. S. Ogando *et al.*, The enzymatic activity of the nsp14 exoribonuclease is critical for replication of MERS-CoV and SARS-CoV-2. *J. Virol.* **94**, e01246-20 (2020).
55. E. Kindler *et al.*, Early endonuclease-mediated evasion of RNA sensing ensures efficient coronavirus replication. *PLoS Pathog.* **13**, e1006195 (2017).
56. X. Deng *et al.*, Coronavirus nonstructural protein 15 mediates evasion of dsRNA sensors and limits apoptosis in macrophages. *Proc. Natl. Acad. Sci. U.S.A.* **114**, E4251–E4260 (2017).
57. C. E. Comar *et al.*, MERS-CoV endoribonuclease and accessory proteins jointly evade host innate immunity during infection of lung and nasal epithelial cells. *Proc. Natl. Acad. Sci. U.S.A.* **119**, e2123208119 (2022).
58. X. Deng *et al.*, Analysis of coronavirus temperature-sensitive mutants reveals an interplay between the macrodomain and papain-like protease impacting replication and pathogenesis. *J. Virol.* **93**, e02140-18 (2019).
59. A. K. Leung *et al.*, Poly(ADP-ribose) regulates stress responses and microRNA activity in the cytoplasm. *Mol. Cell* **42**, 489–499 (2011).
60. Y. Duan *et al.*, PARylation regulates stress granule dynamics, phase separation, and neurotoxicity of disease-related RNA-binding proteins. *Cell Res.* **29**, 233–247 (2019).
61. C. Chiale, T. T. Greene, E. I. Zuniga, Interferon induction, evasion, and paradoxical roles during SARS-CoV-2 infection. *Immunol. Rev.* **309**, 12–24 (2022).
62. M. S. Abers *et al.*, Neutralizing type-I interferon autoantibodies are associated with delayed viral clearance and intensive care unit admission in patients with COVID-19. *Immunol. Cell Biol.* **99**, 917–921 (2021).
63. S. P. Smieszek, V. M. Polymeropoulos, C. Xiao, C. M. Polymeropoulos, M. H. Polymeropoulos, Loss-of-function mutations in IFNAR2 in COVID-19 severe infection susceptibility. *J. Glob. Antimicrob. Resist.* **26**, 239–240 (2021).
64. M. L. Fulcher, S. Gabriel, K. A. Burns, J. R. Yankaskas, S. H. Randell, Well-differentiated human airway epithelial cell cultures. *Methods Mol. Med.* **107**, 183–206 (2005).
65. A. R. Fehr, Bacterial artificial chromosome-based lambda red recombination with the I-scei homing endonuclease for genetic alteration of MERS-CoV. *Methods Mol. Biol.* **2099**, 53–68 (2020).
66. B. K. Tischer, G. A. Smith, N. Osterrieder, En passant mutagenesis: A two step markerless red recombination system. *Methods Mol. Biol.* **634**, 421–430 (2010).
67. L. R. Wong *et al.*, Eicosanoid signalling blockade protects middle-aged mice from severe COVID-19. *Nature* **605**, 146–151 (2022).
68. H. Li *et al.*, The sequence alignment/Map format and SAMtools. *Bioinformatics* **25**, 2078–2079 (2009).
69. H. Thorvaldsdottir, J. T. Robinson, J. P. Mesirov, Integrative genomics viewer (IGV): High-performance genomics data visualization and exploration. *Brief. Bioinform.* **14**, 178–192 (2013).
70. R. Channappanavar, S. Perlman, Evaluation of activation and inflammatory activity of myeloid cells during pathogenic human coronavirus infection. *Methods Mol. Biol.* **2099**, 195–204 (2020).
71. S. Parthasarathy, R. Ghimire, A. Fehr, R. Channappanavar, RNAseq of K18-ACE2 C57BL6 mice lungs infected with SARS-CoV-2 WT strain. Sequence Read Archive (SRA) NCBI. https://www.ncbi.nlm.nih.gov/biosample/?term=SAMN32942675. Deposited 26 January 2023.
72. S. Parthasarathy, R. Ghimire, A. Fehr, R. Channappanavar, RNAseq of K18-ACE2 C57BL6 mice lungs infected with SARS-CoV-2 Mac1 deletion mutant. Sequence Read Archive (SRA) NCBI. https://www.ncbi.nlm.nih.gov/biosample/?term=SAMN32942656. Deposited 26 January 2023.